A&A 414, 141–153 (2004)
DOI: 10.1051/0004-6361:20031634

Astronomy & Astrophysics

Cold dust and molecular gas towards the centers of Magellanic type galaxies and irregulars⋆,⋆⋆

I. The data

M. Albrecht[1], R. Chini[1], E. Krügel[2], S. A. H. Müller[1], and R. Lemke[1]

[1] Astronomisches Institut der Ruhr-Universität Bochum, Universitätsstr. 150, 44780 Bochum, Germany
e-mail: albrecht@astro.rub.de
[2] Max Planck Institut für Radioastronomie Bonn, Auf dem Hügel 69, 53121 Bonn, Germany

Received 29 July 2003 / Accepted 16 October 2003

Abstract. We present 1300 μm continuum emission measurements and observations of the ^{12}CO (1–0) and (2–1) transition towards the centers of 64 Magellanic type galaxies (Sdm/Sm) and irregulars (Im/I0/Irr). The sources are selected to have IRAS flux densities $S_{100\,\mu m} \geq 1000$ mJy and optical diameters mainly below 180″. We were able to detect ^{12}CO towards 41 and the continuum emission towards 28 galaxies. In addition, we obtained the corresponding data for a set of 6 complementary galaxies of different morphological type.

Key words. galaxies: interstellar matter – galaxies: abundances – galaxies: Magellanic type – radio lines: galaxies – radio continuum: galaxies

1. Introduction

Among the various constituents of the interstellar matter (ISM) the amount of dust and molecular gas are decisive quantities for our understanding of galaxy evolution, chemistry and star formation processes. As H_2 lacks a permanent electric dipole moment and its emission arises only from hot or warm gas, absorption measurements against strong far-ultraviolet background sources or indirect methods are used to estimate the mass of the cold molecular component of the ISM. The most widely applied indirect methods consider the CO line emission or the dust mass as tracers. Dust itself is of special interest as it is strongly linked to star formation. It has the property of being very sensitive to the ultraviolet radiation of young massive stars and re-radiates it from infrared to mm wavelengths. A main goal of this study is to obtain measurements of the ^{12}CO line transitions and the continuum emission at 1300 μm at an identical or at least similar spatial resolution. This does not only facilitate a reliable correction of the continuum emission for line contamination but – more importantly – allows a direct comparison of the two independent tracers of the amount of molecular gas.

While similar studies have been conducted for galaxies of Hubble type S0 to Sd (Chini et al. 1996; Krügel et al. 1988a, 1988b, 1990), no systematic approach to observe dust as well as molecular gas towards Magellanic type dwarfs with the same beam size has been made so far. The presented measurements will allow a comparison with galaxies of earlier Hubble type as regards their properties derived from mm observations.

In the following we describe the observational setups and the data reduction. We present the resulting flux densities of the 1300 μm continuum emission. Furthermore, we show the obtained ^{12}CO spectra and list the corresponding line parameters. For a set of galaxies the ^{12}CO lines led to independent distance estimates which in conjunction with data from the literature were used to newly derive H I and optical properties of the objects. The data will be discussed in detail elsewhere (Albrecht et al., in prep.).

2. Galaxy sample

Our galaxy sample contains 31 Magellanic type spirals (Sdm, Sm), 30 Magellanic irregulars (Im) and 3 irregulars (I0, Irr) according to the classification of de Vaucouleurs et al. (1991, hereafter RC3). The objects have been taken from the compilation of morphological dwarf galaxies with known optical magnitudes, optical sizes and H I fluxes by

Send offprint requests to: M. Albrecht,
e-mail: albrecht@astro.rub.de

⋆ Based on observations collected at ESO, La Silla, Chile and IRAM, Pico Veleta, Spain.

⋆⋆ The full version of Figs. 3 and 4 is only available in electronic form at http://www.edpsciences.org

Table 1. The Sdm/Sm sample.

Name	Name	RA (J2000.0)	Dec (J2000.0)	D	Angular Size	d_{25}	$S_{100\,\mu m}$ (IRAS)	$\log M_{\rm H\,I}$	$M_{\rm B}$	Morph. Type
				[Mpc]	[arcmin]	[kpc]	[mJy]	[$M_\odot$]	[mag]	
(1)	(2)	(3)	(4)	(5)	(6)	(7)	(8)	(9)	(10)	(11)
NGC 145	ARP 19	00:31:45.7	−05:09:10	55.0 (P)	1.8 × 1.3	28.8	6156	9.97	–20.9	SB(s)dm
NGC 178	IC 39,	00:39:08.5	−14:10:17	19.3 (P)	2.0 × 1.0	11.2	2586	9.40	–18.8	SB(s)m
NGC 959	UGC 2002	02:32:24.0	+35:29:42	10.1 (c)	2.3 × 1.4	6.8	2709	8.49	–17.8	Sdm:
IC 292	IC 1887	03:10:12.9	+40:45:56	39.8 (H)	1.2 × 0.6	13.9	4617	9.50	–19.6	Sdm
DDO 36		05:07:46.9	−16:17:37	27.0 (H)	2.3 × 1.4	18.1	1528	9.57	–19.0	SB(s)m
UGCA 103	DDO 230	05:10:47.0	−31:35:50	12.8 (H)	3.0 × 2.5	11.2	1413	9.12	–17.5	SB(r)dm
NGC 1879	UGCA 110	05:19:48.2	−32:08:34	16.3 (P)	2.5 × 1.7	11.9	1079	9.04	–18.1	SB(s)m
UGC 4151		08:04:18.7	+77:49:00	30.7 (P)	1.4 × 1.3	12.5	2220	8.97	–19.4	Sdm:
NGC 2537	UGC 4274	08:13:14.7	+45:59:26	5.9 (f)	1.7 × 1.5	2.9	4810	8.23	–16.8	SB(s)m pec
NGC 2730	UGC 4743	09:02:15.9	+16:50:18	51.3 (P)	1.7 × 1.3	25.4	1996	9.67	–20.3	SBdm:
NGC 3057	UGC 5404	10:05:39.1	+80:17:08	20.4 (H)	2.2 × 1.3	13.1	1397	9.06	–18.3	SB(s)dm
NGC 3246	UGC 5661	10:26:41.8	+03:51:43	28.6 (H)	2.4 × 1.3	20.0	1574	9.67	–19.5	SABdm
NGC 3445	UGC 6021	10:54:35.9	+56:59:24	27.3 (P)	1.6 × 1.5	12.7	2960	9.50	–19.3	SAB(s)m
NGC 3659	UGC 6405	11:23:45.4	+17:49:06	17.4 (P)	2.1 × 1.1	10.6	4073	9.28	–18.7	SB(s)m?
NGC 3664	UGC 6419	11:24:25.0	+03:19:34	18.4 (P)	2.0 × 1.9	10.7	1962	9.27	–18.4	SB(s)m pec
NGC 3839	UGC 6700	11:43:54.3	+10:47:06	78.9 (H)	1.0 × 0.5	23.0	7169	10.24	–20.4	Sdm:
NGC 3879	UGC 6752	11:46:49.8	+69:22:59	19.2 (H)	2.6 × 0.5	14.5	1030	9.24	–18.7	Sdm:
NGC 3991	UGC 6933	11:57:30.4	+32:20:03	42.8 (P)	0.6 × 0.2	7.5	<11 150	10.00	–19.9	Sm
NGC 4234	UGC 7309	12:17:09.2	+03:40:59	20.0 (V)	1.3 × 1.3	7.6	4068	8.50	–18.2	(R')SB(s)m
NGC 4299	UGC 7414	12:21:40.9	+11:30:03	20.0 (V)	1.7 × 1.6	9.9	<8086	9.20	–18.8	SAB(s)dm:
NGC 4523	UGC 7713	12:33:48.0	+15:10:05	20.0 (V)	2.0 × 1.9	11.6	1303	9.26	–17.5	SAB(s)m
IC 3521	UGC 7736	12:34:39.5	+07:09:36	20.0 (V)	1.3 × 0.9	7.6	2301	8.13	–17.6	SBm pec
NGC 4625	IC 3675	12:41:52.6	+41:16:26	8.3 (P)	2.2 × 1.9	5.3	3575	8.71	–16.7	SAB(rs)m pec
NGC 5238	UGC 8565	13:34:42.7	+51:36:51	5.2 (d)	1.7 × 1.4	2.6	1213	7.64	–14.8	SAB(s)dm
DDO 180		13:38:10.3	−09:48:05	17.3 (P)	2.3 × 1.9	11.6	2075	9.14	–18.6	SB(s)m
NGC 5433	UGC 8954	14:02:36.0	+32:30:38	57.5 (H)	1.6 × 0.4	26.8	11 110	9.79	–20.4	Sdm:
NGC 5486	UGC 9036	14:07:25.2	+55:06:11	18.2 (P)	1.9 × 1.2	10.1	1138	9.08	–17.7	SA(s)m:
NGC 5630	UGC 9270	14:27:36.7	+41:15:27	35.6 (H)	2.2 × 0.7	22.8	3536	9.68	–19.8	Sdm:
NGC 6570	UGC 11137	18:11:07.3	+14:05:35	30.7 (H)	1.8 × 1.1	16.1	6250	9.44	–20.1	SB(rs)m:
NGC 7162A		22:00:35.7	−43:08:30	30.3 (H)	2.6 × 2.3	22.9	1122	9.64	–19.1	SB(s)m
UGC 12082	DDO 213	22:34:10.9	+32:51:44	10.8 (H)	2.6 × 2.2	8.2	1911	8.94	–16.3	Sm

Notes: (a): Clemens et al. (1999), (b): Heydari-Malayeri et al. (1990), (c): Ho et al. (1997), (d): Makarova & Karachentsev (1998), (e): Meurer et al. (1994), (f): Sharina et al. (1999), (g): Tikhonov & Karachentsev (1998), (h): Tully (1988), (V): Virgo cluster galaxy, distance from Federspiel et al. (1998), (H): distance from H I velocity of the RC3; (U): distance from optical velocity of the Updated Zwicky Catalogue; (P): present work.

Melisse & Israel (1993a, 1993b). Only galaxies with IRAS flux densities at 100 μm $S_{100\,\mu m} \geq 1000$ mJy according to these authors were taken into account for the present study to yield a sufficient detection probability at mm wavelengths. Moreover, to ensure a considerable coverage of the sources with a single beam size typically of a few ten arcsec for mm observations and concerning technical limitations for the ON–OFF separation only galaxies with a major optical axis at the 25th mag arcsec^{-2} isophote $D_{25} \leq 180''$ were selected. Six galaxies are added to the sample which do not fulfil the size criterion (NGC 1569, NGC 2366, NGC 2976, NGC 3077, NGC 3396 and UGCA 105). Except NGC 3396 these galaxies were chosen because of their high IRAS flux densities at 100 μm and low absolute blue magnitudes which make them especially interesting for a study of morphological dwarf galaxies. NGC 3396 has been taken into account as its major optical axis exceeds the size limit by only 0.1′. Melisse & Israel (1993a, 1993b) explicitly exclude peculiar galaxies according to the morphological classification of de Vaucouleurs et al. (1976, hereafter RC2). Nevertheless, following the classification of the RC3 our sample contains 16 peculiar galaxies. We additionally obtained measurements of the ^{12}CO line and/or

Table 2. The Im/I0/Irr sample.

Name	Name	RA (J2000.0)	Dec (J2000.0)	D	Angular Size	d_{25}	$S_{100\,\mu m}$ (IRAS)	$\log M_{H\,I}$	M_B	Morph. Type
				[Mpc]	[arcmin]	[kpc]	[mJy]	[$M_\odot$]	[mag]	
(1)	(2)	(3)	(4)	(5)	(6)	(7)	(8)	(9)	(10)	(11)
ARP 004	DDO 14	01:48:25.7	−12:22:55	21.5 (H)	2.8 × 2.3	17.5	1601	9.35	–18.0	IAB(rs)m
NGC 899	UGCA 26	02:21:53.1	−20:49:23	20.7 (H)	1.9 × 1.3	11.4	3678	9.86	–18.6	IB(s)m
NGC 1140	Mrk 1063	02:54:33.6	−10:01:40	19.6 (P)	1.7 × 0.9	9.7	3184	9.63	–18.9	IBm pec:
NGC 1602		04:27:53.7	−55:03:26	20.7 (H)	1.9 × 1.1	11.4	1567	9.11	–18.2	IB(s)m pec:
NGC 1569	UGC 3056	04:30:49.0	+64:50:53	2.2 (h)	3.6 × 1.8	2.3	31 748	8.11	–17.3	IBm
UGC 3234	DDO 35	05:03:24.6	+16:24:16	18.7 (H)	1.8 × 1.8	9.8	2505	9.31	–18.0	Im:
UGCA 105		05:14:15.0	+62:34:31	4.0 (h)	5.5 × 3.5	6.4	4710	8.91	–15.7	Im?
NGC 2366	UGC 3851	07:28:54.6	+69:12:57	2.9 (h)	8.1 × 3.3	6.8	4578	8.84	–16.4	IB(s)m
NGC 2415	UGC 3930	07:36:56.4	+35:14:31	50.4 (H)	0.9 × 0.9	13.2	12 890	9.75	–20.9	Im?
NGC 2719	UGC 4718	09:00:15.4	+35:43:40	42.0 (H)	1.3 × 0.3	15.9	2641	10.00	–20.1	Im pec?
NGC 2915		09:26:11.5	−76:37:36	5.3 (e)	1.9 × 1.0	2.9	2120	8.82	–16.3	I0
NGC 3026	UGC 5279	09:50:55.4	+28:33:05	19.8 (H)	2.7 × 0.8	15.6	1339	9.12	–18.4	Im
NGC 3077	UGC 5398	10:03:20.6	+68:44:04	2.1 (h)	5.4 × 4.5	3.3	26 430	8.57	–16.2	I0 pec
UGC 5720	Mrk 33	10:32:31.9	+54:24:03	19.1 (H)	1.0 × 0.9	5.6	5317	8.63	–18.0	Im pec
NGC 3396	UGC 5935	10:49:55.2	+32:59:27	22.4 (P)	3.1 × 1.2	20.2	16 800	9.69	–19.4	IBm pec
UGC 6345	DDO 94	11:20:15.6	+02:31:31	21.3 (H)	2.3 × 1.3	14.3	1851	9.47	–18.3	IB(s)m
NGC 3738	UGC 6565	11:35:48.8	+54:31:26	4.3 (h)	2.5 × 1.9	3.1	2405	8.15	–16.2	Irr
NGC 4032	UGC 6995	12:00:32.9	+20:04:26	20.0 (V)	1.9 × 1.8	11.1	1547	9.25	–18.9	Im:
NGC 4190	UGC 7232	12:13:44.7	+36:38:03	3.5 (g)	1.7 × 1.5	1.7	1262	7.78	–14.4	Im pec
NGC 4194	UGC 7241	12:14:09.7	+54:31:38	33.5 (H)	1.8 × 1.1	17.5	25 880	9.28	–19.8	IBm pec
NGC 4485	UGC 7648	12:30:31.1	+41:42:01	8.0 (H)	2.3 × 1.6	5.4	<3730	8.68	–17.3	IB(s)m pec
UGC 7690		12:32:26.8	+42:42:18	7.3 (H)	1.7 × 1.6	3.6	1209	8.42	–15.9	Im:
IC 3476	UGC 7695	12:32:41.9	+14:03:00	20.0 (V)	2.1 × 1.8	12.2	2384	8.66	–18.7	IB(s)m:
NGC 4532	UGC 7726	12:34:19.3	+06:28:07	20.0 (V)	2.9 × 1.1	16.9	16 210	9.75	–19.6	IBm
NGC 4630	UGC 7871	12:42:31.2	+03:57:32	20.0 (V)	1.8 × 1.3	10.5	4189	8.88	–18.5	IB(s)m?
NGC 4810	UGC 8034	12:54:51.2	+02:38:25	12.1 (U)	1.9 × 0.8	6.7	1213	–	–16.1	Im pec
UGC 8303	DDO 166	13:13:17.6	+36:13:03	12.7 (H)	2.2 × 1.9	8.1	1420	8.75	–17.0	IAB(s)m
NGC 5408		14:03:21.0	−41:22:44	4.9 (h)	1.6 × 0.8	2.3	2157	8.63	–16.8	IB(s)m
NGC 5464		14:07:04.4	−30:01:01	35.9 (H)	1.3 × 0.8	13.6	2964	9.81	–19.9	IB(s)m?
ARP 261	DDO 197	14:49:30.6	−10:10:24	24.6 (H)	3.0 × 2.0	21.5	2799	9.65	–19.1	IB(s)m pec
NGC 5798	UGC 9628	14:57:37.9	+29:58:06	24.1 (P)	1.4 × 1.0	9.8	2260	8.99	–18.5	Im:
IC 4662		17:47:06.4	−64:38:25	2.0 (b)	2.8 × 1.6	1.6	11 230	8.13	–15.2	IBm
NGC 7292	UGC 12048	22:28:25.8	+30:17:33	13.5 (P)	2.1 × 1.7	8.2	2725	8.96	–18.0	IBm

Notes: See Table 1.

Table 3. The complementary sample.

Name	Name	RA (J2000.0)	Dec (J2000.0)	D	Angular Size	d_{25}	$S_{100\,\mu m}$ (IRAS)	$\log M_{H\,I}$	M_B	Morph. Type
				[Mpc]	[arcmin]	[kpc]	[mJy]	[$M_\odot$]	[mag]	
(1)	(2)	(3)	(4)	(5)	(6)	(7)	(8)	(9)	(10)	(11)
NGC 1012	UGC 2141	02:39:14.9	+30:09:06	12.9 (P)	2.5 × 1.1	9.4	8464	9.36	–18.3	S0/a?
UGCA 116	IIZw40	05:55:42.6	+03:23:30	10.0 (P)	0.6 × 0.2	1.7	<19 720	8.70	–17.1	Sbc
NGC 2976	UGC 5221	09:47:15.3	+67:55:00	2.1 (h)	5.9 × 2.7	3.6	29 710	7.82	–16.3	SAc pec
UGCA 247	DDO 239	11:48:45.8	−28:17:41	25.6 (P)	2.5 × 2.2	18.6	3131	9.63	–19.5	SB(s)d:
NGC 7107		21:42:26.5	−44:47:25	29.3 (H)	2.0 × 1.5	17.0	1534	9.38	–19.3	SB(rs)cd
NGC 7732	UGC 12738	23:41:34.0	+03:43:29	39.0 (P)	1.9 × 0.6	21.6	2231	10.03	–19.6	Scd pec sp

Notes: See Table 1.

continuum emission towards 6 complementary galaxies of different morphological type. In the following we have divided the complete set of observed galaxies into three sub-samples: Magellanic type spirals (Sdm/Sm), irregulars and Magellanic type irregulars (Im/I0/Irr) and the sample of complementary sources. The name, alternative name and coordinates of the galaxies are given in Tables 1–3 for the corresponding subsamples. To estimate the distances to the sources the heliocentric radial velocities based on H I observations have been extracted from the NASA/IPAC Extragalactic Database (NED)[1] and have been converted to velocities with respect to the local standard of rest $v_{\rm lsr}$. The radial velocity of NGC 4810 is based on optical observations from the RC3. In case of a ^{12}CO detection with a single Gauss component the central velocity of the ^{12}CO line (see Sect. 4.1) is used instead. For galaxies with $v_{\rm lsr} > 600\,{\rm km\,s^{-1}}$ the distances have been derived using a Hubble constant of $H_0 = 75\,{\rm km\,s^{-1}\,Mpc^{-1}}$. The distances to galaxies with $v_{\rm lsr} \leq 600\,{\rm km\,s^{-1}}$ have been taken from the literature as identified in the notes to Table 1. Eight galaxies of the sample are members of the Virgo cluster, for which a mean distance of 20.0 Mpc is assumed (Federspiel et al. 1998) without applying Virgo-centric infall corrections. Column (5) of Tables 1–3 lists the adopted distances.

3. Observations and data reduction

The observations of the ^{12}CO (1–0) and (2–1) line transitions and the 1300 μm continuum emission were obtained at the IRAM 30 m telescope (MRT) and the 15 m Swedish ESO Submillimeter Telescope (SEST) between 1997 and 2002. The telescopes provide beam sizes (HPBW) of 45″ (SEST) and 24″ (MRT) at 115 GHz and 24″ (SEST) and 11″ (MRT) at 230 GHz.

3.1. ^{12}CO line emission

At the SEST a balanced ON–OFF dual beam switching mode was applied with a separation between the ON and OFF beams of 11′50″ in azimuth at a frequency of 6 Hz. The dual channel 115/230 GHz SIS receiver was tuned to the central H I velocity in each source. Spectra were obtained with two acousto optical spectrometers (LR1 and LR2) providing 1440 channels each and a width of 0.7 MHz per channel. The total bandwidth available was 1 GHz at both backends, yielding a velocity resolution of 1.8 km s^{-1} and 0.9 km s^{-1} for ^{12}CO (1–0) and (2–1), respectively. Pointing and focus were checked before each integration about every two hours on bright SiO masers and planets. The pointing accuracy was found to be always better than 5″ in azimuth and elevation. Regular calibrations were performed using the standard chopper wheel method (Ulich & Haas 1976). System temperatures usually varied between 300 K and 500 K, infrequently rising higher due to bad weather conditions.

[1] This research has made use of the NASA/IPAC Extragalactic Database (NED) which is operated by the Jet Propulsion Laboratory, California Institute of Technology, under contract with the National Aeronautics and Space Administration.

Table 4. Velocity resolution for those cases differing from 10 km s^{-1}.

Name	Telescope	^{12}CO transition	δv [km s^{-1}]
NGC 2730	MRT	2–1	12
	SEST	1–0	15
NGC 3664	MRT	1–0	13
	MRT	2–1	12
NGC 5486	MRT	2–1	13
NGC 7732	MRT	1–0	21
	SEST	1–0	15

At the MRT a wobbler switching mode was performed at a frequency of 0.5 Hz with a beam throw between 150″ and 240″ in azimuth depending on the size of the source. Two 3 mm SIS receivers (A100, B100) and two 1.3 mm SIS receivers (A230, B230) were used to observe both polarisations of the ^{12}CO (1–0) and (2–1) transitions simultaneously. The 3 mm SIS receivers were connected to a low resolution filter-bank with a total bandwidth of 1 GHz and a resolution of 1 MHz. The filter-bank was split into two parts with 512 channels for each receiver. As backend for the 1.3 mm SIS receivers an auto-correlator was used providing a bandwidth of 512 MHz and 409 channels with a resolution of 1.25 MHz for each receiver. This yields a velocity resolution of 2.6 km s^{-1} and 1.6 km s^{-1} for ^{12}CO (1–0) and (2–1), respectively. Pointing and focus were checked before each integration about every two hours on continuum sources and planets. The pointing accuracy was found to be always better than 4″ in azimuth and elevation. Calibrations were performed frequently using the chopper wheel method. System temperatures usually varied between 200 K and 400 K, again infrequently rising higher due to bad weather conditions.

All obtained spectra were reduced using the CLASS software package[2] (Buisson et al. 1997). Multiple scans were averaged weighted by a factor of $t/T_{\rm sys}^2$, where t is the integration time and $T_{\rm sys}$ the system temperature of the individual scans. Scans showing nonlinear baselines or artificial features were rejected. The intensity scale of the resulting spectra in corrected antenna temperature $T_{\rm A}^*$ was converted to main beam brightness temperature $T_{\rm mb}$. From the averaged spectra linear baselines were subtracted. All spectra were boxcar-smoothed to a resolution of $\delta v = 10\,{\rm km\,s^{-1}}$. In a few cases spectra were smoothed to lower resolutions to receive a better signal-to-noise ratio as given in Table 4. For all spectra where a molecular line was detected, a Gauss function was fitted to determine the central velocity and velocity width and to check the signal-to-noise ratio S/N. Spectra clearly showing more than one velocity component were fitted using up to three Gaussians.

In case of $S/N \geq 3$, the velocity integrated ^{12}CO line intensity $I = \int T_{\rm mb}\,{\rm d}v$ was determined by numerical integration of the smoothed spectra within the limits set by the line. The errors were calculated according to Elfhag et al. (1996): Assuming a perfect baseline, the line uncertainty is given by

$$\Delta I_{\rm l} = \sigma \sqrt{n}\,\delta v, \qquad (1)$$

[2] The CLASS package is part of the GILDAS software. The manual can be retrieved via the IRAM web-page.

where σ is the rms noise per channel, n the number of channels covered by the line and δv the velocity resolution per channel. For linear baselines the baseline fitting uncertainty can be determined as

$$\Delta I_{\rm b} = \sigma\, n\, \delta v\, \sqrt{\frac{1}{N-n}}\,, \tag{2}$$

where N is the total number of channels in the spectra. This results in a total error of the integrated ^{12}CO line intensities given by

$$\Delta I = \sqrt{\Delta I_{\rm l}^2 + \Delta I_{\rm b}^2} = \sigma\, \delta v\, \sqrt{n + \frac{n^2}{N-n}}. \tag{3}$$

Assuming uncorrelated channel-to-channel fluctions we have calculated upper limits in case of non-detections ($S/N < 3$) as

$$I < 3\,\sigma\, \sqrt{\Delta v_{\rm tot}(^{12}{\rm CO})\, \delta v}, \tag{4}$$

where $\Delta v_{\rm tot}(^{12}$CO) is the expected total velocity width of the ^{12}CO line, which is not actually obtained. To derive secure upper limits for I we use the full velocity width of the H I line at 20% or 50% maximum power multiplied by 1.69 or 2.58, respectively, as an upper limit for $\Delta v_{\rm tot}(^{12}$CO). Δv_{20}(H I) and Δv_{50}(H I) are taken from the RC3. In case of a Gaussian shape of the H I spectrum this would result in the full H I velocity width at 1% of the maximum power: Δv_1(H I) = 1.69 Δv_{20}(H I) or Δv_1(H I) = 2.58 Δv_{50}(H I). To inspect the reliability of this approach we have compared the resulting values for Δv_1(H I) with the total velocity width $\Delta v_{\rm tot}(^{12}$CO) for those cases where a clear detection ($S/N \geq 3$) was obtained. Figure 1 shows the ratio of $\Delta v_{\rm tot}(^{12}$CO) to Δv_1(H I) as a function of projected beam size, where $\Delta v_{\rm tot}(^{12}$CO) is determined from the smoothed spectra. All ^{12}CO detections, i.e. both transitions and both telescopes, irrespective of the number of fitted Gaussians are displayed. Except for the extreme case of NGC 4194 all galaxies posess values for the ratio $\Delta v_{\rm tot}(^{12}{\rm CO})/\Delta v_1$(H I) below one showing that Δv_1(H I) can be used as a secure approximation for $\Delta v_{\rm tot}(^{12}$CO) in case of non-detections.

Figure 1 shows the tendency of increasing ^{12}CO line width normalised on the H I width with increasing coverage of the source by a single beam. This can be expected as the ^{12}CO beam resolves a galaxy while the H I width refers to the entire object. Evidently, beam projection effects play a key role in analysing the data presented here and will be a major topic in the subsequent discussion (see Paper II). Especially the question arises, what fraction of the total flux is detected.

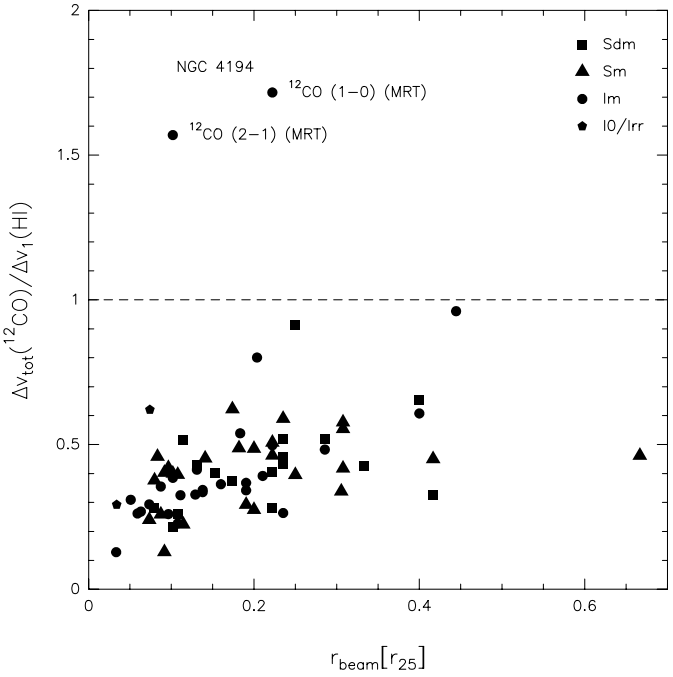

Fig. 1. Ratio of the total ^{12}CO velocity width to the H I velocity width at 1% of the maximum power versus the projected beam size in units of the optical radius. All ^{12}CO detections (i.e. both transitions and both telescopes) are displayed. The dashed line denotes equality.

3.2. 1300 μm continuum emission

Observations of the 1300 μm continuum emission at the MRT were carried out using the MPIfR 37-channel bolometer array (Kreysa 1990; Thum et al. 1992). Each channel of the array has a half power beam width of 11″. The channels are arranged in a hexagonal structure with a pixel-to-pixel separation of 23″. A filter set coupled to the atmospheric window provides a bandwidth of 50 GHz around a central wavelength of 1250 μm. All observations were made in a symmetrical ON–OFF mode with a beam separation between 70″ and 120″ in azimuth and a wobbling frequency of 0.51 Hz. Integration times varied between 30 min and 2 hours per source. Due to the Nasmyth-system the bolometer array rotates with respect to the source as a function of hour angle and elevation. To ensure that the channel positions with respect to the galaxy do not move, the integrations were conducted during those time intervals when the rotation of the array had its minimum. Pointing and focus were checked before each integration about every two hours on strong continuum sources and planets. The pointing accuracy was found to be mostly better than 4″ in azimuth and elevation. To obtain the atmospheric opacity the sky emission was measured regularly at a number of elevation angles.

At the SEST the continuum observations were carried out using a single channel bolometer of the MPIfR. The characteristics of this bolometer are similar to the individual elements of the array used at the MRT. It provides a bandwidth of about 50 GHz centered at a wavelength of 1270 μm. A dual beam switching mode (ON–OFF) with a separation of 120″ between the ON- and OFF-beam was applied for all observations. Again pointing and focus were checked before each integration about every two hours on strong continuum sources and planets and the atmospheric opacity was determined regularly. The pointing accuracies are similar to those at the MRT.

The reduction of single-channel data is straightforward and consists mainly of baseline subtraction and weighted averaging. On the other hand the use of multiple channels provides the opportunity of correlated sky-noise suppression and the subtraction of mean background emission. We have developed a

reduction software package in the framework of NIC[3] providing a sophisticated sky-noise suppression and the selection of arbitrary channels for the background determination. As a result signal-to-noise ratios increased by about 10–15% in comparison to the values provided by common software could be achieved for most observations.

4. Results

4.1. ^{12}CO line emission

Of a total of 67 galaxies observed ^{12}CO was detected in 41 sources (Sdm/Sm: 21, Im/I0/Irr: 15, complementary sample: 5) yielding detection rates of 72% and 47% for the Sdm/Sm and Im/I0/Irr subsample, respectively. Figure 3 shows the spectra taken at the MRT and Fig. 4 those taken at the SEST at a resolution of 10 km s^{-1} (for exceptions see Table 4). The results are presented in Table 5, where Col. (1) gives the object name and Col. (2) identifies the ^{12}CO transition. The parameters of the Gaussian fits are listed in Cols. (3)–(5) for the MRT and Cols. (8)–(10) for the SEST observations, where Cols. (3) and (8) give the central velocities with respect to the local standard of rest, Cols. (4) and (9) the line width (FWHM) and Cols. (5) and (10) the peak values of the main beam brightness temperature. In case the spectrum is fit by more than one Gaussian, the parameters of all components are listed. The rms noise per channel is contained in Cols. (6) and (11) and the velocity integrated line intensity including the total error or the corresponding upper limit is given in Cols. (7) and (12). All values correspond to a velocity resolution of 10 km s^{-1} except for those cases stated in Table 4.

4.2. 1300 μm continuum emission

Of a total of 52 galaxies observed the continuum emission at 1300 μm has been detected towards 28 sources (Sdm/Sm: 9, Im/I0/Irr: 16, complementary sample: 3) resulting in detection rates of 47% and 57% for the Sdm/Sm and Im/I0/Irr subsample, respectively. In Table 6 the results are listed, where Col. (1) identifies the name, Cols. (2)–(7) refer to MRT and Cols. (8)–(10) to SEST observations. The flux density from the central channel of the multi-channel array at the MRT is given in Col. (2), where for signal-to-noise ratios $S/N < 3$ upper limits are given quantified as three times the rms noise. The corresponding errors refer to the signal noise solely and do not include the calibration uncertainty which was determined to be 16%. In case signal-to-noise ratios $S/N \geq 3$ were reached for channels apart from the central one we have summed up the corresponding flux densities including the center position. The values are given in Col. (3) and Col. (4) lists the total number of the mentioned channels. In Col. (8) the flux density resulting from the single-channel bolometer at the SEST is given, where the calibration uncertainty of 21% again is not included in the total error.

The thermal continuum emission observed at 1300 μm is affected by contamination from molecular lines. The strongest lines emitted within the bolometer bandwidth are ^{12}CO(2–1), ^{13}CO(2–1), C^{18}O(2–1) and CS(5–4). According to Braine et al. (1995) the line contribution is given by

$$S_{\rm line} = \frac{2\,k}{\lambda^3\,\Delta f}\,\frac{2\,\pi\,\theta^2}{8\,\ln 2}\,I \qquad (5)$$

where k is the Boltzmann constant, λ the wavelength, Δf the bandwidth, θ the half power beam width (HPBW) of the bolometer and I the velocity integrated line intensity. For a bandwidth of $\Delta f = 50$ GHz and a beam size of $\theta = 11''$ at the MRT and $\theta = 24''$ at the SEST this leads to a contribution of the ^{12}CO(2–1) line of $S_{^{12}\mathrm{CO(2-1)}} = 0.081\,I_{\mathrm{CO(2-1)}}$ at the MRT and $S_{^{12}\mathrm{CO(2-1)}} = 0.386\,I_{\mathrm{CO(2-1)}}$ at the SEST, where $S_{^{12}\mathrm{CO(2-1)}}$ is given in mJy and $I_{^{12}\mathrm{CO(2-1)}}$ in K km s^{-1}. We were able to determine the line contribution for 14 galaxies with a mean of 11 ± 10%. The values are listed in Cols. (3) and (9). In case no exact value could be derived we used the mean contribution to correct for line contamination except for those cases where the upper limits are not in accordance with the mean (MRT: NGC 3839, ARP 261; SEST: NGC 899, NGC 1140, NGC 1602, NGC 5464). In these cases we used the individual upper limits as a more reliable approximation for the correction. Apart from ^{12}CO(2–1) no other lines have been taken into consideration as they account for a much lower contribution (Braine et al. 1995). The corrected flux densities of the central channel at the MRT, the sum of all channels of the array with $S/N \geq 3$ and the single-channel at the SEST are given in Cols. (6), (7) and (10), respectively.

Figure 2 shows the fractional line contamination versus the projected beam size. Opposite to Fig. 1 no dependency is apparent. Both, CO and 1300 μm continuum, refer to the same

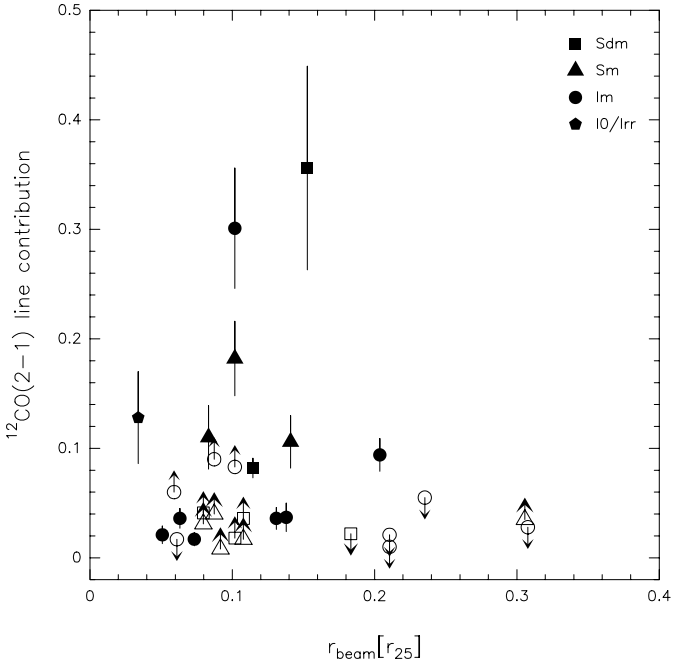

Fig. 2. Fractional ^{12}CO(2–1) line contribution to the 1300 μm continuum emission versus the projected beam size in units of the optical radius. Vertical bars mark the rms of the individual values. Open symbols denote upper or lower limits.

[3] The NIC package is part of the GILDAS software. The manual can be retrieved via the IRAM web-page.

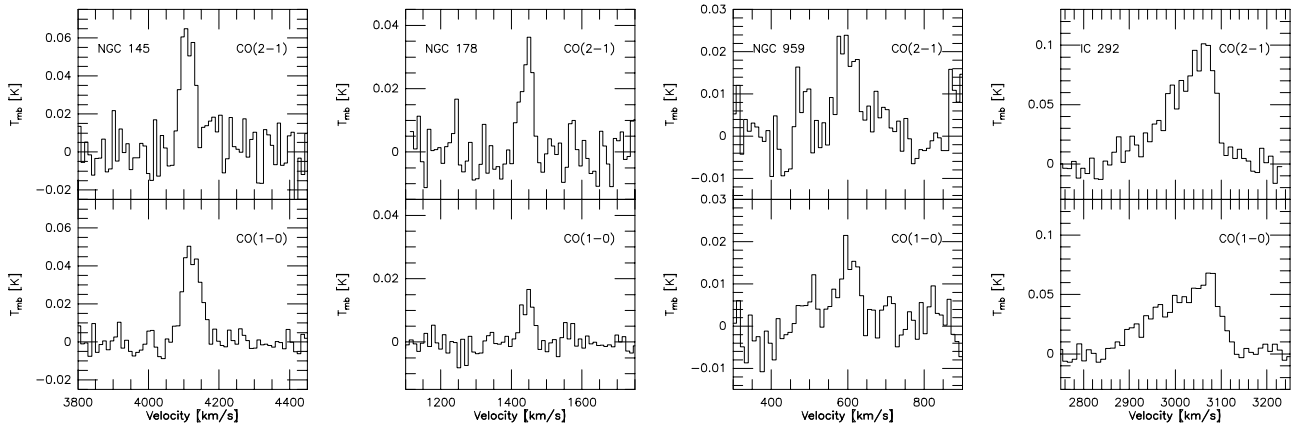

Fig. 3. ^{12}CO (1–0) and (2–1) spectra from MRT for NGC 145, NGC 178, NGC 959 and IC 292. The full version of Fig. 3 is available at `http://www.edpsciences.org`.

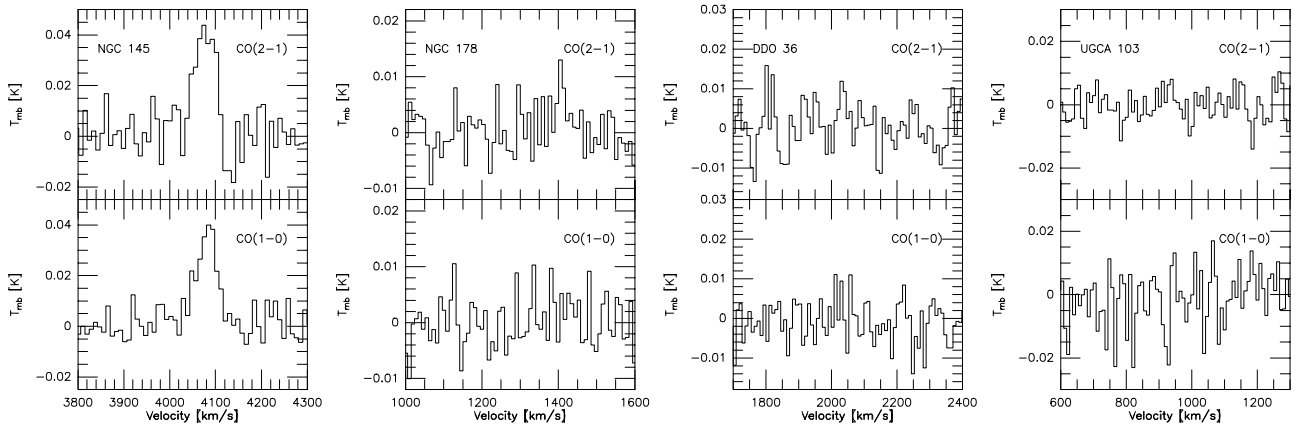

Fig. 4. ^{12}CO (1–0) and (2–1) spectra from SEST for NGC 145, NGC 178, DDO 36 and UGCA 103. The full version of Fig. 4 is available at `http://www.edpsciences.org`.

beam size. Nevertheless, a systematic difference in the spatial distribution of ^{12}CO and dust would be reflected in the plot. Again we refer to Paper II for a more precise discussion of this topic. The scatter in the diagram cannot be attributed to measurement errors alone and has to be intrinsic to the galaxies.

4.3. H I and optical data

We were able to independently determine the radial velocity using the ^{12}CO observations resulting in new distance values for a set of galaxies for which the spectra can be fit with a single Gaussian component. The adopted distances given in Tables 1–3 were used to newly derive H I and optical properties.

To estimate the amount of atomic hydrogen in the sample galaxies the H I line magnitudes m_{21} have been taken from the RC3. The H I line magnitude is defined as

$$m_{21} = 16.6 - 2.5 \log S_{\rm H\,I}, \quad (6)$$

where the H I flux $S_{\rm H\,I}$ is in units of 10^{-22} W m^{-2}. The values of $S_{\rm H\,I}$ for IC 292 and NGC 7732 are taken from Schneider et al. (1992) corrected and mirrored according to Melisse & Israel (1993a). No H I data are available for NGC 4810. From this the apparent H I mass in solar units $M_{\rm H\,I}$ corrected for redshift z is given by

$$\log M_{\rm H\,I} = \log S_{\rm H\,I} + \log(1+z) + 2 \log D + 5.696, \quad (7)$$

where the distance D is in units of Mpc (de Vaucouleurs et al. 1991). The self-absorption of the H I flux as a function of axis ratio is still an object of debate. To retrieve the true H I mass, we have applied the suggestion of de Vaucouleurs et al. (1991) to correct the H I magnitude by $m^0_{21} = m_{21} - 0.5 \log R_{25}$ for all galaxies with morphological type parameters $T \geq 1$, where the major-to-minor axis ratio R_{25} is set to 10.0 for all galaxies with $R_{25} \geq 10.0$. The resulting values for the H I mass are given in Col. (9) of Tables 1–3.

The angular size (major and minor axis) of the galaxies at the 25th mag arcsec^{-2} isophote as taken from the NED is mirrored in Col. (6) of Tables 1–3. This enables the calculation of the absolute linear diameter which is listed in Col. (7) of the same tables.

To derive the absolute blue magnitude $M_{\rm B}$, the total blue magnitude $B^0_{\rm T}$ corrected for galactic absorption, internal absorption and redshift has been extracted from the RC3. The values for UGCA 116 and NGC 4810 are taken from Tully (1988) and the value for NGC 2719 is taken from Kraan-Korteweg (1986). Using the adopted distances the

Table 5. Results of the ^{12}CO observations from MRT and SEST.

		MRT					SEST				
Name	^{12}CO	v_{LSR} [km s^{-1}]	dv [km s^{-1}]	T_{mb} [mK]	σ_{rms} [mK]	$I_{^{12}CO}$ [K km s^{-1}]	v_{LSR} [km s^{-1}]	dv [km s^{-1}]	T_{mb} [mK]	σ_{rms} [mK]	$I_{^{12}CO}$ [K km s^{-1}]
(1)	(2)	(3)	(4)	(5)	(6)	(7)	(8)	(9)	(10)	(11)	(12)
Sdm / Sm											
NGC 145	1–0	4122	58	49.6	4.7	3.05 ± 0.19	4081	53	38.1	4.9	2.14 ± 0.17
	2–1	4111	45	65.1	10.7	2.87 ± 0.32	4076	48	45.8	8.3	2.26 ± 0.27
NGC 178	1–0	1446	38	14.8	2.8	0.60 ± 0.09	–	–	–	4.5	<0.49
	2–1	1445	37	34.0	6.2	1.29 ± 0.18	–	–	–	4.2	<0.46
NGC 959	1–0	601	63	16.5	4.8	1.11 ± 0.21					
	2–1	599	59	21.2	6.3	1.29 ± 0.24					
IC 292	1–0	2994	152	42.4	5.8	9.32 ± 0.39					
		3074	55	45.5	5.8						
	2–1	3014	126	60.0	8.2	11.00 ± 0.59					
		3067	46	63.4	8.2						
DDO 36	1–0	–	–	–	4.2	<0.37	–	–	–	4.6	<0.38
	2–1	–	–	–	7.2	<0.62	–	–	–	6.7	<0.56
UGCA 103	1–0						–	–	–	8.8	<1.22
	2–1						–	–	–	5.5	<0.77
NGC 1879	1–0	–	–	–	6.2	<0.92	–	–	–	13.6	<1.88
	2–1	1219	56	17.2	6.1	0.90 ± 0.18	–	–	–	12.8	<1.78
UGC 4151	1–0	2297	91	32.6	2.7	3.05 ± 0.12					
	2–1	2297	77	39.5	5.1	3.04 ± 0.21					
NGC 2537	1–0	443	56	15.7	3.1	0.91 ± 0.13					
	2–1	447	47	19.3	4.5	0.94 ± 0.15					
NGC 2730	1–0	3847	97	18.8	2.7	1.95 ± 0.14	3760	148	8.8	2.9	1.37 ± 0.24
	2–1	3846	69	16.3	5.4	1.21 ± 0.23	3743	103	11.2	3.5	1.20 ± 0.18
NGC 3057	1–0	–	–	–	3.0	<0.45					
	2–1	–	–	–	5.1	<0.75					
NGC 3246	1–0	–	–	–	3.5	<0.71	–	–	–	3.9	<0.73
	2–1	–	–	–	4.0	<0.79	–	–	–	4.7	<0.89
NGC 3445	1–0	2045	41	21.0	3.0	0.94 ± 0.10					
	2–1	2048	23	24.6	7.2	0.50 ± 0.18					
NGC 3659	1–0	1303	86	44.0	4.7	3.92 ± 0.21	–	–	–	6.1	<1.15
	2–1	1311	67	46.3	5.7	3.25 ± 0.25	–	–	–	3.6	<0.68
NGC 3664	1–0	1383	39	6.6	2.1	0.29 ± 0.08	–	–	–	6.5	<0.79
	2–1	1385	14	16.9	4.2	0.27 ± 0.08	–	–	–	5.5	<0.67
NGC 3839	1–0	5827	79	28.5	2.6	5.47 ± 0.20					
		5926	66	21.4	2.6						
		6018	71	19.2	2.6						
	2–1	–	–	–	9.1	<2.06					
NGC 3879	1–0	–	–	–	3.6	<0.66					
	2–1	–	–	–	6.9	<1.24					

absolute blue magnitude of the galaxies has been determined following

$$M_B = B_T^0 - 5 \log D - 25\,, \quad (8)$$

where the distance D is in units of Mpc (de Vaucouleurs et al. 1991). The results are given in Col. (10) of Tables 1–3.

Acknowledgements. Part of this project was supported by the Deutsche Forschungsgemeinschaft (DFG) via the Graduiertenkolleg *The Magellanic Clouds and other Dwarf Galaxies*.

Table 5. continued.

		MRT					SEST				
Name	^{12}CO	v_{LSR} [km s^{-1}]	dv [km s^{-1}]	T_{mb} [mK]	σ_{rms} [mK]	$I_{^{12}CO}$ [K km s^{-1}]	v_{LSR} [km s^{-1}]	dv [km s^{-1}]	T_{mb} [mK]	σ_{rms} [mK]	$I_{^{12}CO}$ [K km s^{-1}]
(1)	(2)	(3)	(4)	(5)	(6)	(7)	(8)	(9)	(10)	(11)	(12)
NGC 3991	1–0	3210	96	16.7	3.3	1.63 ± 0.15					
	2–1	3206	42	45.0	4.7	2.79 ± 0.19					
		3255	31	21.4	4.7						
NGC 4234	1–0	2051	47	58.6	11.7	2.85 ± 0.44	–	–	–	15.8	<2.25
	2–1	–	–	–	14.1	<2.09	–	–	–	15.9	<2.29
NGC 4299	1–0	222	44	13.6	4.1	0.52 ± 0.16					
	2–1	–	–	–	10.3	<1.53					
NGC 4523	1–0	–	–	–	3.8	<0.57					
	2–1	–	–	–	5.4	<0.79					
IC 3521	1–0	586	55	72.7	4.6	4.30 ± 0.17	–	–	–	10.7	<1.42
	2–1	584	44	102.2	13.4	4.75 ± 0.45	588	52	41.8	8.2	2.09 ± 0.29
NGC 4625	1–0	620	42	84.7	5.5	3.61 ± 0.17					
	2–1	627	33	119.8	12.6	4.31 ± 0.37					
DDO 180	1–0	1296	39	33.0	3.9	1.38 ± 0.14					
	2–1	1297	32	33.1	6.3	1.09 ± 0.17					
NGC 5433	1–0	4233	126	48.9	4.8	20.30 ± 0.54					
		4385	315	42.0	4.8						
	2–1	4298	160	65.2	12.6	19.31 ± 1.05					
		4214	97	82.3	12.6						
NGC 5486	1–0	–	–	–	2.5	<0.44					
	2–1	1368	79	9.5	3.1	0.82 ± 0.16					
NGC 6570	1–0	2246	95	40.0	3.8	6.38 ± 0.22	2200	28	16.8	5.1	2.28 ± 0.27
		2347	94	26.4	3.8		2309	138	13.7	5.1	
	2–1	2279	105	59.2	5.5	7.93 ± 0.32	2198	32	9.3	5.5	2.63 ± 0.32
		2366	41	31.6	5.5		2329	117	18.8	5.5	
NGC 7162A	1–0						–	–	–	3.4	<0.46
	2–1						–	–	–	5.5	<0.75
UGC 12082	1–0	–	–	–	1.7	<0.18					
	2–1	–	–	–	3.0	<0.32					
Im / I0 / Irr											
ARP 004	1–0	–	–	–	3.8	<0.52					
	2–1	–	–	–	7.2	<0.95					
NGC 899	1–0	–	–	–	4.3	<0.63	–	–	–	3.4	<0.46
	2–1	–	–	–	9.4	<1.34	–	–	–	4.1	<0.56
NGC 1140	1–0	1473	42	18.9	4.3	0.97 ± 0.17	–	–	–	6.5	<1.14
	2–1	1475	55	46.4	6.1	2.82 ± 0.22	–	–	–	7.4	<1.32
NGC 1602	1–0						–	–	–	3.3	<0.37
	2–1						–	–	–	2.3	<0.26

Table 5. continued.

		MRT					SEST				
Name	^{12}CO	v_{LSR}	dv	T_{mb}	σ_{rms}	$I_{^{12}CO}$	v_{LSR}	dv	T_{mb}	σ_{rms}	$I_{^{12}CO}$
		[km s^{-1}]	[km s^{-1}]	[mK]	[mK]	[K km s^{-1}]	[km s^{-1}]	[km s^{-1}]	[mK]	[mK]	[K km s^{-1}]
(1)	(2)	(3)	(4)	(5)	(6)	(7)	(8)	(9)	(10)	(11)	(12)
NGC 1569	1–0	–71	31	30.3	3.8	1.08 ± 0.10					
	2–1	–70	22	55.4	5.5	1.38 ± 0.14					
UGC 3234	1–0	–	–	–	3.5	<0.71	–	–	–	5.2	<0.73
	2–1	–	–	–	4.0	<0.79	–	–	–	5.4	<0.77
UGCA 105	1–0	–	–	–	2.1	<0.30					
	2–1	107	14	11.2	3.0	0.31 ± 0.06					
NGC 2366	1–0	–	–	–	2.6	<0.34					
	2–1	–	–	–	3.5	<0.45					
NGC 2415	1–0	3750	88	89.8	5.7	12.78 ± 0.34					
		3833	72	58.7	5.7						
	2–1	3730	79	110.0	10.5	16.70 ± 0.61					
		3791	112	64.9	10.5						
NGC 2719	1–0	–	–	–	1.4	<0.34					
	2–1	–	–	–	3.5	<0.81					
NGC 2915	1–0						–	–	–	8.8	<1.28
	2–1						–	–	–	4.9	<0.72
NGC 3026	1–0	–	–	–	2.6	<0.48					
	2–1	–	–	–	11.6	<2.10					
NGC 3077	1–0	–1	32	158.0	10.2	5.32 ± 0.35					
	2–1	–2	23	195.9	18.1	4.77 ± 0.41					
UGC 5720	1–0	1405	31	22.4	3.2	3.99 ± 0.15					
		1456	67	45.3	3.2						
	2–1	1404	32	51.4	5.7	4.98 ± 0.26					
		1460	57	55.0	5.7						
NGC 3396	1–0	1683	46	56.1	3.5	2.87 ± 0.14					
	2–1	1682	40	92.8	10.2	4.39 ± 0.36					
UGC 6345	1–0	–	–	–	3.8	<0.56					
	2–1	–	–	–	6.7	<0.96					
NGC 3738	1–0	224	22	19.9	2.3	0.51 ± 0.07					
	2–1	227	25	23.6	4.6	0.58 ± 0.11					
NGC 4032	1–0	1271	43	19.6	3.1	0.86 ± 0.11					
	2–1	1264	43	19.3	3.3	0.83 ± 0.09					
NGC 4190	1–0	–	–	–	6.3	<0.64					
	2–1	–	–	–	18.4	<1.83					
NGC 4194	1–0	2480	86	75.9	3.4	29.26 ± 0.26					
		2569	129	143.1	3.4						
		2683	44	55.3	3.4						
	2–1	2475	104	138.7	7.6	45.45 ± 0.65					
		2570	112	214.9	7.6						
		2680	43	104.7	7.6						

Table 5. continued.

		MRT					SEST				
Name	^{12}CO	$v_{\rm LSR}$ [km s^{-1}]	dv [km s^{-1}]	$T_{\rm mb}$ [mK]	$\sigma_{\rm rms}$ [mK]	$I_{^{12}{\rm CO}}$ [K km s^{-1}]	$v_{\rm LSR}$ [km s^{-1}]	dv [km s^{-1}]	$T_{\rm mb}$ [mK]	$\sigma_{\rm rms}$ [mK]	$I_{^{12}{\rm CO}}$ [K km s^{-1}]
(1)	(2)	(3)	(4)	(5)	(6)	(7)	(8)	(9)	(10)	(11)	(12)
NGC 4485	1–0	–	–	–	3.1	<0.50					
	2–1	–	–	–	8.1	<1.28					
UGC 7690	1–0	–	–	–	3.1	<0.38					
	2–1	–	–	–	3.3	<0.40					
IC 3476	1–0	−144	46	55.9	4.6	2.80 ± 0.16					
	2–1	−147	40	76.2	12.5	3.60 ± 0.44					
NGC 4532	1–0	2044	61	37.0	3.5	2.34 ± 0.14	–	–	–	5.5	<0.99
	2–1	2042	49	62.1	7.3	3.25 ± 0.26	2037	66	20.3	4.1	1.39 ± 0.15
NGC 4630	1–0	735	58	66.2	7.0	3.86 ± 0.33					
	2–1	737	72	70.0	19.8	4.84 ± 0.81					
NGC 4810	1–0	–	–	–	3.0	$<0.029\sqrt{\Delta v}$					
	2–1	–	–	–	3.7	$<0.035\sqrt{\Delta v}$					
NGC 5408	1–0						–	–	–	4.9	<0.56
	2–1						–	–	–	4.1	<0.47
NGC 5464	1–0						–	–	–	5.3	<0.88
	2–1						–	–	–	4.5	<0.75
ARP 261	1–0	–	–	–	4.0	<0.68	–	–	–	5.7	<0.89
	2–1	–	–	–	8.0	<1.30	–	–	–	6.2	<0.98
NGC 5798	1–0	1806	93	10.7	2.3	1.05 ± 0.12					
	2–1	1796	88	15.9	3.2	1.36 ± 0.16					
IC 4662	1–0						–	–	–	5.5	<0.70
	2–1						–	–	–	3.2	<0.42
NGC 7292	1–0	1010	18	23.0	5.0	0.38 ± 0.14	–	–	–	9.4	<1.05
	2–1	–	–	–	2.8	<0.33	–	–	–	7.2	<0.81
complementary galaxies											
NGC 1012	1–0	968	68	40.5	7.3	2.95 ± 0.30					
	2–1	964	59	105.0	8.3	6.35 ± 0.29					
UGCA 116	1–0	752	28	6.1	1.8	0.23 ± 0.05	–	–	–	6.1	<0.92
	2–1	750	39	15.7	2.2	0.69 ± 0.07	–	–	–	6.6	<1.01
NGC 2976	1–0	−4	31	121.0	5.3	4.12 ± 0.17					
	2–1	−1	22	90.4	13.2	1.98 ± 0.30					
UGCA 247	1–0						1918	55	18.3	3.4	1.13 ± 0.13
	2–1						1928	41	13.9	3.1	0.62 ± 0.10
NGC 7107	1–0						–	–	–	2.3	<0.27
	2–1						–	–	–	2.9	<0.34
NGC 7732	1–0	2925	87	21.6	7.0	1.96 ± 0.39	2921	79	7.7	2.6	0.58 ± 0.14
	2–1	2956	130	46.1	10.9	5.92 ± 0.57	2923	98	9.1	3.0	0.95 ± 0.13

Table 6. Results of the continuum observations from MRT and SEST.

	MRT						SEST		
Name	$S_{1300\ \mu m}$ [mJy]	$S_{^{12}CO}/S_{1300\ \mu m}$ [%]	$\Sigma S_{1300\ \mu m}$ [mJy]	Number of Chans.	S_{dust} [mJy]	ΣS_{dust} [mJy]	$S_{1300\ \mu m}$ [mJy]	$S_{^{12}CO}/S_{1300\ \mu m}$ [%]	S_{dust} [mJy]
(1)	(2)	(3)	(4)	(5)	(6)	(7)	(8)	(9)	(10)
Sdm / Sm									
NGC 145	<12.9	>2	–	0	<11.6	–			
NGC 959	<2.4	>4	–	0	<2.2	–			
IC 292	2.5 ± 0.6	36	2.5 ± 0.6	1	1.6 ± 0.5	1.6 ± 0.5			
UGCA 103							<12.5	–	<11.2
NGC 1879							<8.4	–	<7.5
NGC 2537	<4.8	>2	6.5 ± 1.4	1	<4.3	5.8 ± 1.5			
NGC 2730	<2.8	>4	–	0	<2.5	–			
NGC 3246	<6.0	–	–	0	<5.4	–			
NGC 3659	<6.4	>4	–	0	<5.7	–	<12.6	–	<11.2
NGC 3664	<2.4	>1	–	0	<2.2	–			
NGC 3839	5.8 ± 1.7	<2	5.8 ± 1.7	1	5.7 ± 1.6	5.7 ± 1.6			
NGC 3991	<6.6	>4	–	0	<5.9	–			
NGC 4299	<4.6	–	6.8 ± 2.0	1	<4.1	6.1 ± 1.9	<7.2	–	<6.5
IC 3521	3.6 ± 0.7	11	24.3 ± 6.4	7	3.2 ± 0.7	21.7 ± 5.8			
NGC 4625	3.1 ± 0.8	11	50.0 ± 8.4	9	2.8 ± 0.7	44.5 ± 7.6			
NGC 5238	<1.9	–	–	0	<1.7	–			
DDO 180	<2.9	>3	18.9 ± 5.3	5	<2.6	16.9 ± 5.1	<7.4	–	<6.6
NGC 5433	19.0 ± 1.8	8	92.0 ± 17.8	10	17.4 ± 1.7	84.4 ± 16.4			
NGC 6570	3.5 ± 0.6	18	6.1 ± 1.3	2	2.9 ± 0.5	5.0 ± 1.1			
Im / I0 / Irr									
ARP 004							<23.4	–	<20.9
NGC 899	<3.0	–	–	0	<2.7	–	10.6 ± 1.9	<2	10.4 ± 1.9
NGC 1140							9.2 ± 3.1	<6	8.7 ± 2.9
NGC 1602							9.7 ± 2.6	<1	9.6 ± 2.6
NGC 1569	5.2 ± 1.7	2	18.3 ± 5.6	3	5.1 ± 1.7	17.9 ± 5.5			
UGC 3234	<4.6	–	–	0	<4.1	–			
NGC 2415	14.3 ± 2.2	9	14.3 ± 2.2	1	13.0 ± 2.0	13.0 ± 2.0			
NGC 2915							<13.1	–	<11.7
NGC 3077	3.1 ± 1.0	13	3.1 ± 1.0	1	2.7 ± 0.9	2.7 ± 0.9			
NGC 3396	<6.03	>6	4.8 ± 1.6	1	<5.4	4.3 ± 1.5			
UGC 6345							<14.6	–	<13.0
NGC 3738	2.9 ± 0.9	2	7.7 ± 2.3	2	2.9 ± 0.9	7.6 ± 2.3			
NGC 4032							<14.3	–	<12.7
NGC 4190	<2.9	–	–	0	<2.63	–			
NGC 4194	12.2 ± 2.2	30	12.2 ± 2.2	1	8.5 ± 1.7	8.5 ± 1.7			
NGC 4485	<2.1	–	7.3 ± 1.9	2	<1.9	6.5 ± 1.8			
UGC 7690	<2.6	–		0	<2.3	–			
IC 3476	<3.2	>9	5.6 ± 1.2	1	2.9 ± 1.0	5.0 ± 1.2			
NGC 4532	7.3 ± 1.8	4	7.3 ± 1.8	1	7.0 ± 1.7	7.0 ± 1.7	14.5 ± 4.8	4	13.9 ± 4.7
NGC 4630	<4.7	>8	–	0	<4.2	–			
NGC 4810	<3.0	–	–	0	<2.7	–			

Table 6. continued.

	MRT						SEST		
Name	$S_{1300\,\mu m}$ [mJy]	$S_{^{12}CO}/S_{1300\,\mu m}$ [%]	$\Sigma S_{1300\,\mu m}$ [mJy]	Number of Chans.	S_{dust} [mJy]	ΣS_{dust} [mJy]	$S_{1300\,\mu m}$ [mJy]	$S_{^{12}CO}/S_{1300\,\mu m}$ [%]	S_{dust} [mJy]
(1)	(2)	(3)	(4)	(5)	(6)	(7)	(8)	(9)	(10)
UGC 8303	<2.9	–	3.7 ± 0.9	1	<2.6	3.3 ± 0.9			
NGC 5408							<5.3	–	<4.8
NGC 5464							10.5 ± 3.0	<3	10.2 ± 2.9
ARP 261	6.4 ± 2.1	<2	16.1 ± 4.4	2	6.3 ± 2.0	15.8 ± 4.3	<14.8	–	<13.2
NGC 5798	3.0 ± 0.8	4	16.0 ± 4.4	5	2.9 ± 0.8	15.4 ± 4.3			
IC 4662							<8.6	–	<7.7
NGC 7292	<3.6	–	–	0	<3.3				
complementary galaxies									
NGC 1012	6.7 ± 2.1	8	6.7 ± 2.1	1	6.2 ± 2.0	6.2 ± 2.0			
UGCA 116	13.3 ± 3.1	1	13.3 ± 3.1	1	13.3 ± 3.1	13.3 ± 3.1			
NGC 2976	<2.0	>8	22.7 ± 5.4	7	<1.8	20.3 ± 5.4			
UGCA 247							<9.2	>3	<8.2
NGC 7107							<6.0	–	<5.4

References

Braine, J., Krügel, E., Sievers, A., & Wielebinski, R. 1995, A&A, 295, L55

Buisson, G., Desbats, L., Duvert, G., et al. 1997, Continuum and Line Analysis Single-dish Software, Observatoire de Grenoble and IRAM

Chini, R., Krügel, E., & Lemke, R. 1996, A&AS, 118, 47

Clemens, M. S., Alexander, P., & Green, D. A. 1999, MNRAS, 307, 481

de Vaucouleurs, G., de Vaucouleurs, A., & Corwin, H. G. 1976, Second Reference Catalogue of Bright Galaxies (Austin: University of Texas Press)

de Vaucouleurs, G., de Vaucouleurs, A., Corwin, et al. 1991, Third Reference Catalogue of Bright Galaxies (New York: Springer)

Elfhag, T., Booth, R. S., Höglund, B., Johansson, L. E. B., & Sandqvist, A. 1995, A&AS, 115, 439

Federspiel, M., Tammann, G. A., & Sandage, A. 1998, ApJ, 495, 115

Heydari-Malayeri, M., Melnick, J., & Martin, J.-M. 1990, A&A, 234, 99

Ho, L. C., Fillipenko, A. V., & Sargent, W. L. W. 1997, ApJS, 112, 315

Kraan-Korteweg, R. C. 1986, A&AS, 66, 255

Kreysa, E. 1990, in Proc. 29th Liège International Astrophysical Colloq., From Ground-Based to Space-Borne Sub-mm Astronomy (ESA SP-314), ed. J.-P. Swings, & D. Fraipont (Noordwijk: ESA Publications Division), 265

Krügel, E., Chini, R., Kreysa, E., & Sherwood, W. A. 1988a, A&A, 190, 47

Krügel, E., Chini, R., Kreysa, E., & Sherwood, W. A. 1988b, A&A, 193, L16

Krügel, E., Steppe, H., & Chini, R. 1990, A&A, 229, 17

Makarova, L. N., & Karachentsev, I. D. 1998, A&AS, 133, 181

Melisse, J. P. M., & Israel, F. P. 1993a, A&AS, 103, 391

Melisse, J. P. M., & Israel, F. P. 1993b, A&A, 285, 51

Meurer, G. R., Mackie, G., & Carignan, C. 1994, AJ, 107, 2021

Schneider, S. E., Thuan, T. X., Mangum, J. G., & Miller, J. 1992, ApJS, 81, 5

Sharina, M. E., Karachentsev, I. D., & Tikhonov, N. A. 1999, AstL, 25, 322

Tikhonov, N. A., & Karachentsev, I. D. 1998, A&AS, 128, 325

Thum, C., Kreysa, E., & John, D. 1992, IRAM Working Report No. 212, IRAM, Grenoble

Tully, B. R. 1988, Nearby Galaxies Catalog (Cambridge: Cambridge University Press)

Ulich, B. L., & Haas, R. W. 1976, ApJS, 30, 247

Online Material

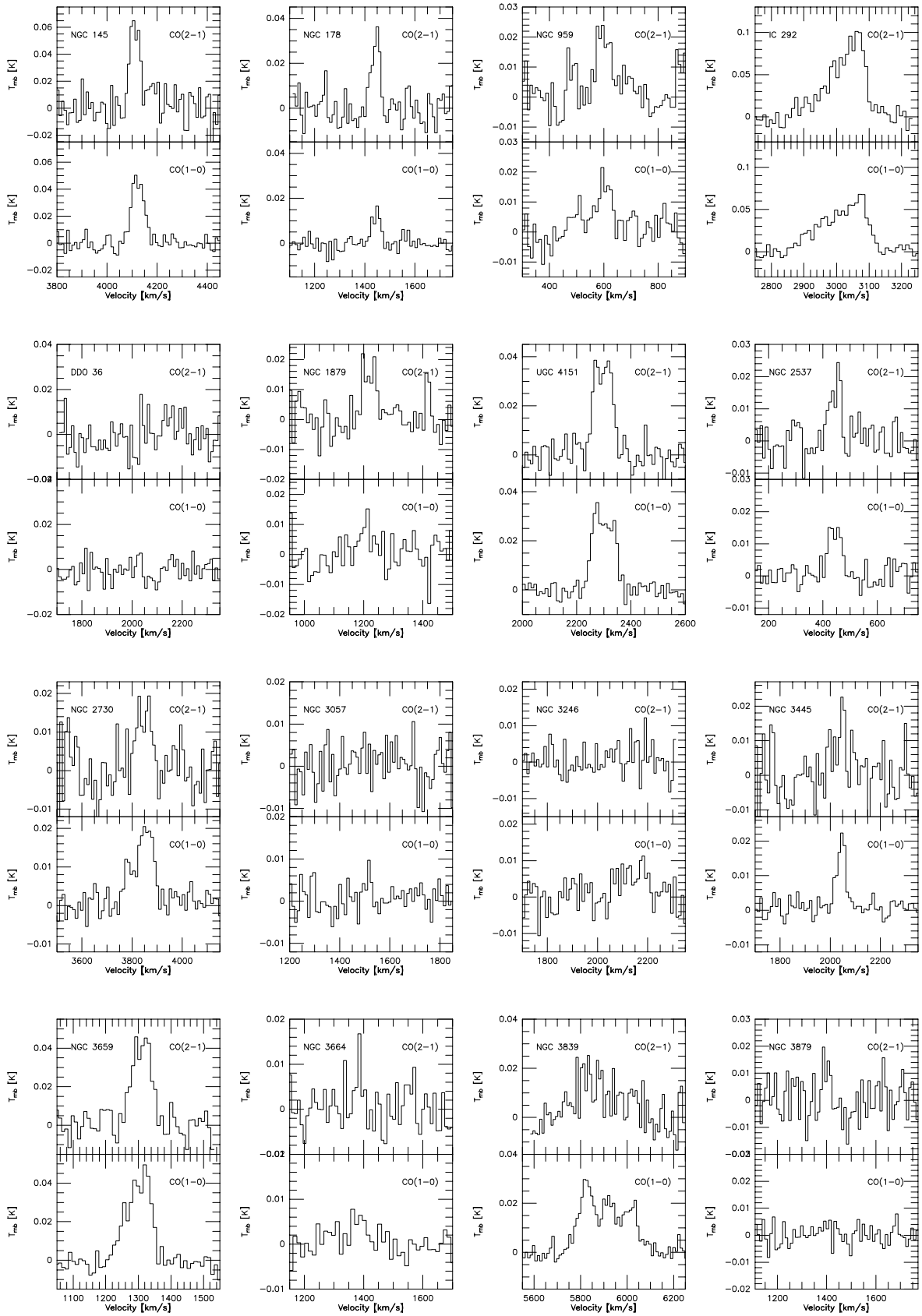

Fig. 3. continued.

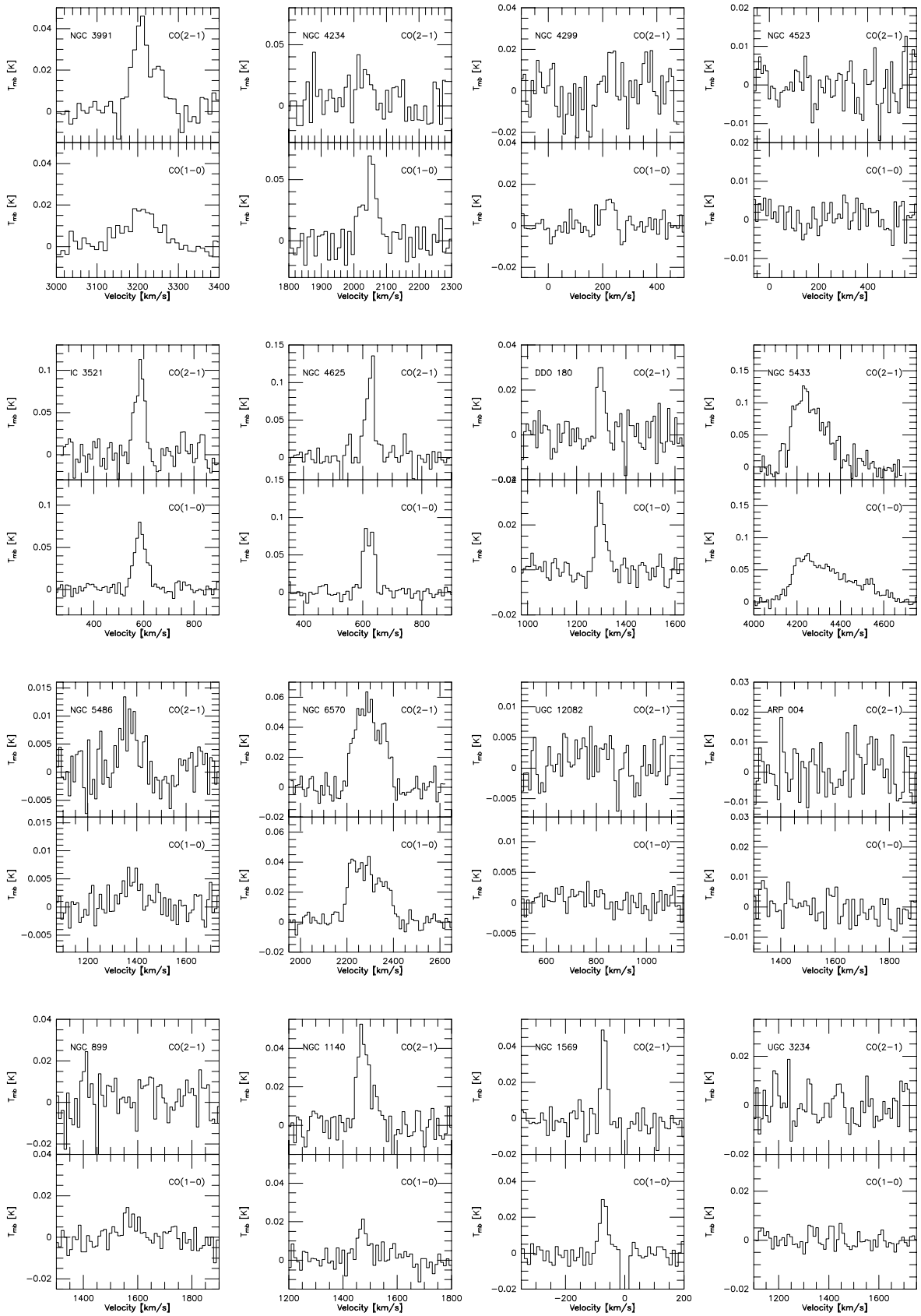

Fig. 3. continued.

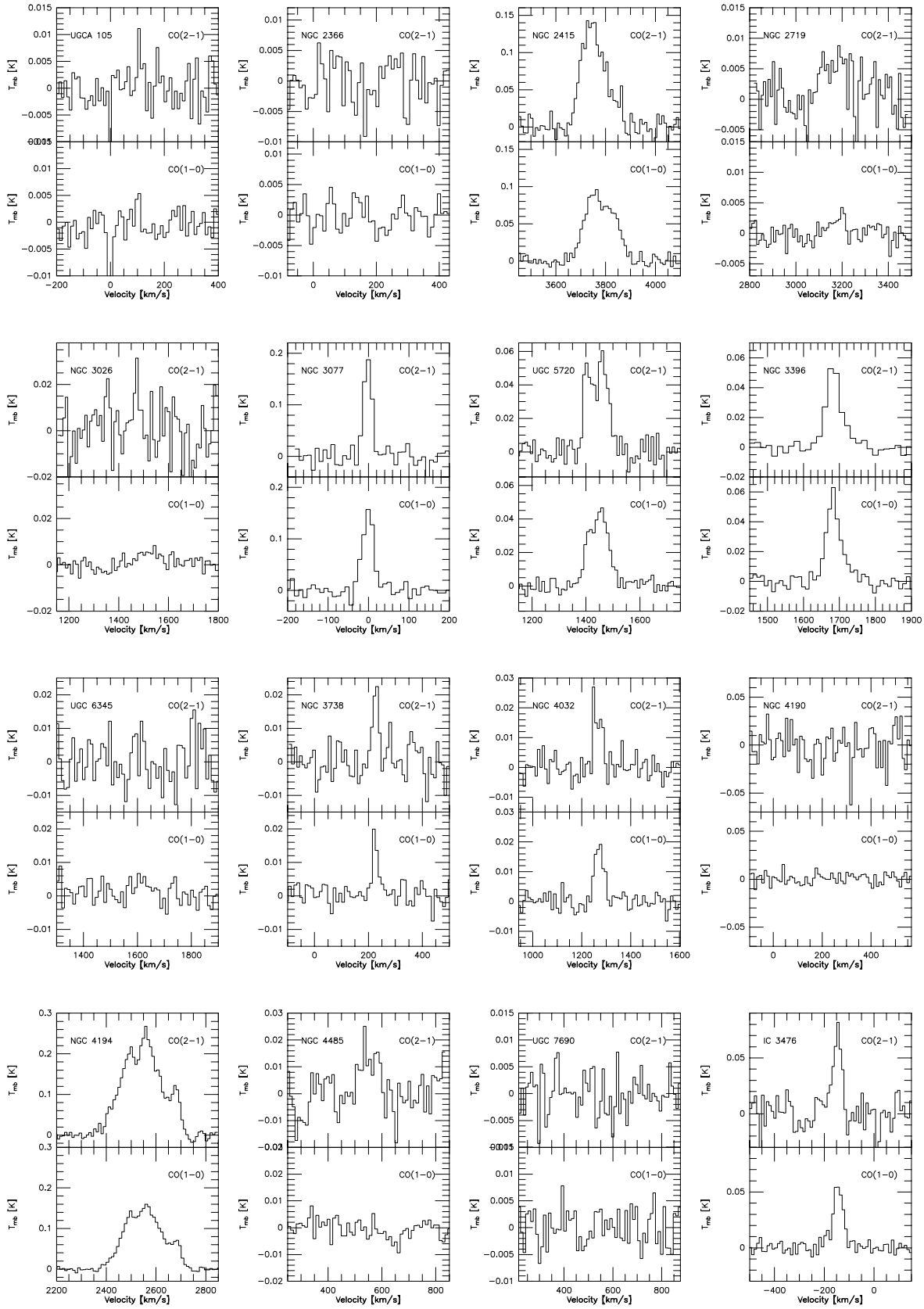

Fig. 3. continued.

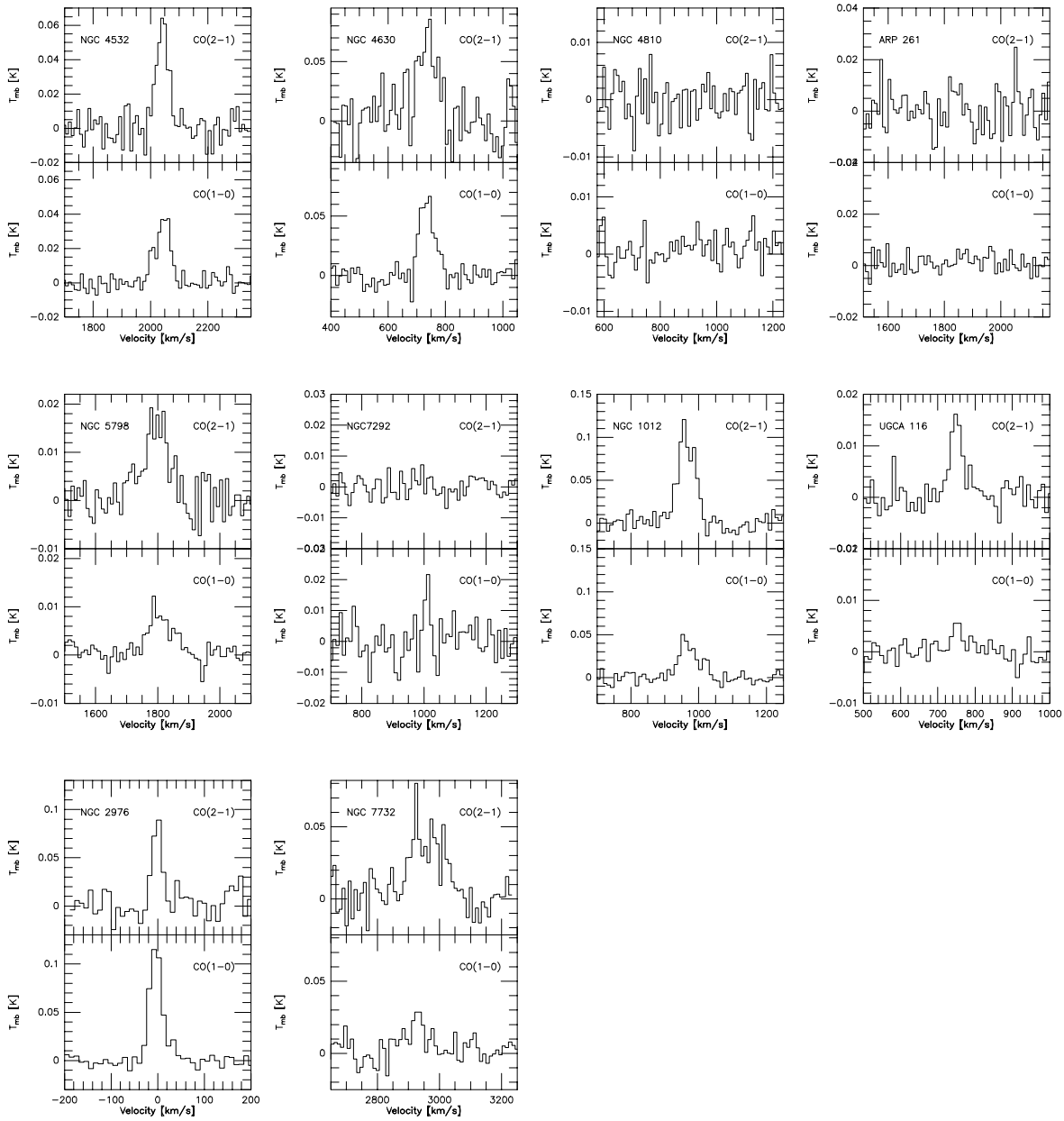

Fig. 3. continued.

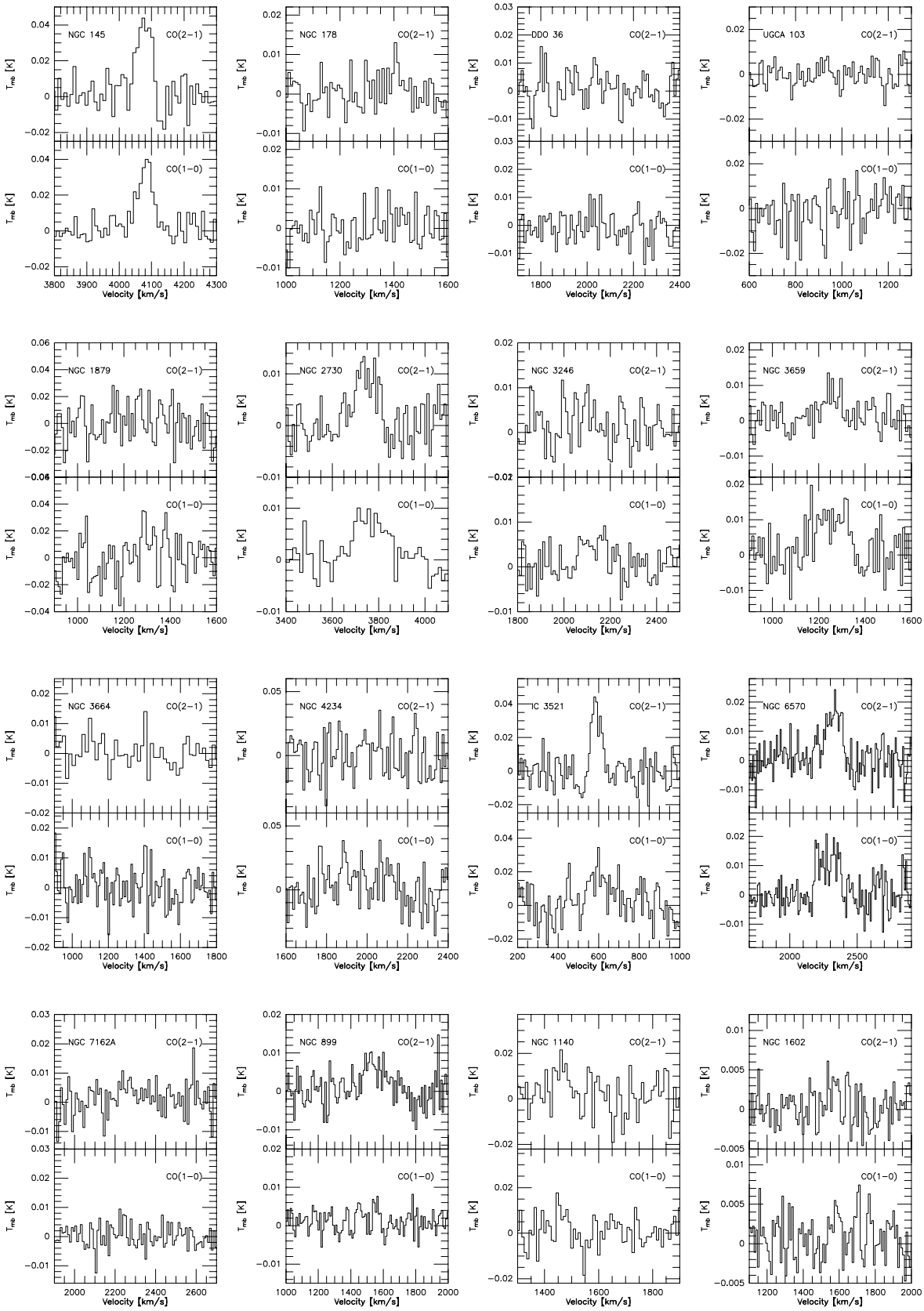

Fig. 4. continued.

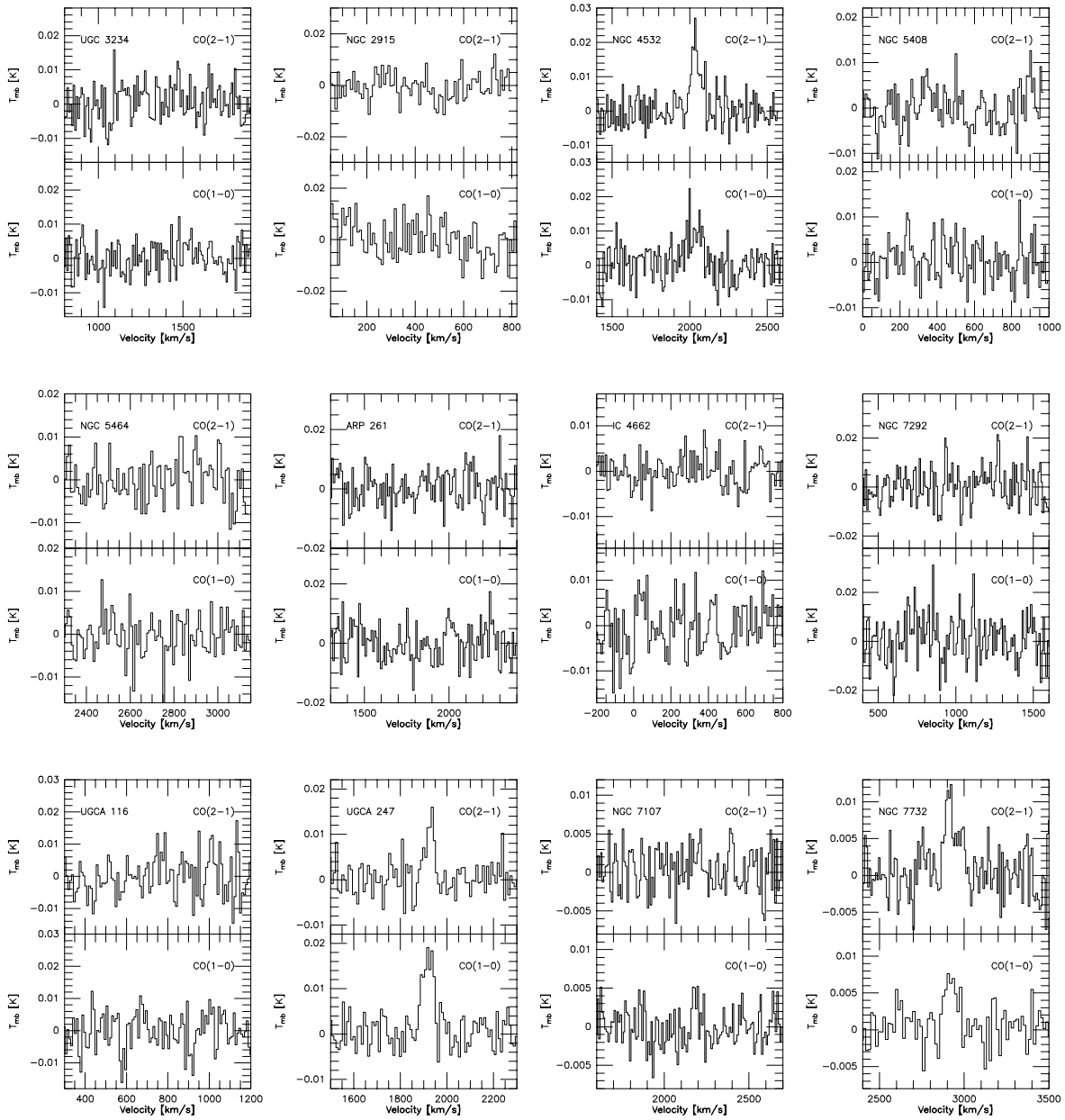

Fig. 4. continued.